Numerical dissipation of flux splitting schemes for contact discontinuities

Jun Liu (liujun65@dlut.edu.cn)
Dalian University of Technology
Fang Han
Dalian University of Technology
Yan Xin Wei
Dalian University of Technology

Research

Keywords: Flux splitting schemes, Numerical dissipation, Contact discontinuity, Numerical experiments, Non-physical error interference

DOI: https://doi.org/10.21203/rs.3.rs-499376/v1

Numerical dissipation of flux splitting schemes for contact discontinuities

Jun Liu*, Fang Han, and Yan-Xin Wei
*Correspondence: liujun65@dlut.edu.cn
School of Aeronautic and Astronautics, Dalian University of Technology , 116024 Dalian, China

Abstract

The contact discontinuity is simulated by three kinds of flux splitting schemes to evaluate and analyse the influence of numerical dissipation in this paper. The numerical results of one-dimensional contact discontinuity problem show that if the flow velocity on both sides of the contact discontinuity is not simultaneously supersonic, the non-physical pressure and velocity waves may occur when the initial theoretically contact discontinuity is smeared into a transition zone spanning several grid-cells caused by numerical dissipations. Since these non-physical waves have no effect on the corresponding density dissipation, this paper considers these fluctuations as only numerical errors and are not part of the numerical dissipation. In addition, for two-dimensional flow field, the characteristics of high-order accuracy difference schemes, i.e. low dissipation and high resolution, may induce the multi-dimensional non-physical waves that interfere with each other to produce more complex non-physical flow structures, so the fluctuations in the calculated results should be treated with caution.

Keywords: Flux splitting schemes, Numerical dissipation, Contact discontinuity, Numerical experiments, Non-physical error interference

1 Introduction

In Computational Fluid Dynamics(CFD), numerical dissipation is considered to derive from the truncation error introduced by the discrete convection term of the spatial discrete schemes, which is closely related to the computational accuracy and stability of the scheme. CFD researchers often use the method of reducing numerical dissipation to construct higher precision computational schemes[1-3]. The spatial discrete scheme consists of two parts, the difference scheme and the flux splitting scheme, and this paper mainly discusses the numerical dissipation characteristics of the flux splitting scheme, while the upwind scheme, as the mainstream scheme for solving convective fluxes in CFD at present[4], becomes the object of study in this paper.

The upwind schemes are divided into three categories: the Flux Vector Splitting (FVS) scheme, the Flux Difference Splitting (FDS) scheme, and the hybrid scheme. At present, the main viewpoints of CFD on the numerical dissipation of upwind schemes are as follows[5]. The simplification strategy used by FVS scheme represented by Steger-Warming scheme[6] and VanLeer scheme[7] leads to excessive numerical

dissipation and reduces the simulation accuracy of viscous flow. The FDS scheme represented by Roe scheme[8] and HLLC scheme[9] are based on solving the local Riemannian problem with low numerical dissipation, which makes the FDS schme able to accurately capture nonlinear and linear waves such as shock waves and contact discontinuties, while the computational stability at strong shock waves is poor, such as the "Carbuncle" phenomenon of the Roe scheme. The hybrid schme, as a combination of the above two schemes, has both the robustness of FVS scheme for nonlinear wave capture and the high resolution of FDS scheme for linear wave capture, with lower dissipation than FVS scheme and better stability than FDS scheme, such as AUSM+ scheme[10], LDFSS scheme[11], etc.

After examining the above literature, we still have the following questions about the numerical dissipation of the flux splitting scheme. First, the numerical dissipation of the difference scheme has specific mathematical definitions and expressions according to the modified equation in the CFD field, which is expressed as the even power derivative term of the modified equation. However, there is no precise definition and calculation formula for the numerical dissipation of the flux splitting scheme, and the so-called dissipation magnitude in some literature for constructing low dissipation flux splitting schemes is only a qualitative interpretation based on the numerical results, and no quantitative evaluation criterion has been seen so far. Therefore, whether numerical dissipation exists in the flux splitting scheme, and if so, how to define it becomes the first question in this paper. Besides, among the above three kinds of flux splitting schemes, it is generally believed that the FVS scheme has the largest numerical dissipation without optimization, and why the numerical dissipation of the FVS scheme is larger than that of the FDS and hybrid schemes is the second question of this paper.

The classical examples for verifying the dissipation size of the scheme values are Sod[12], Lax[13], Shu-Osher[14] and 2-D Riemann problem[15], in which the initial discontinuity often contains a complex Riemann structure and it is difficult to distinguish which structure the computational error comes from or is caused by the interference of different structures. The above three kinds of flux splitting schemes were used in the literature [16] and [17] to simulate a moving positive shock wave with the Mach number $M_s = 3$, and the computational results show that no matter which flux splitting scheme is used, an isentropic wave and a non-isentropic wave are generated downstream of the shock during the formation of the numerical transition region from the initial mathematical discontinuity. The results in references [18] and [19] also show that the non-physical waves generated by the shock-capturing method to calculate the moving positive shock will contaminate the

downstream region of the shock and change the structure distribution of the flow field, which brings difficulties to the data analysis.

Therefore, the simpler contact discontinuity problems are chosen for the study in this paper, and the rest of the paper is organized as follows. In Section 2, the computational results are presented for different flux splitting schemes for contact discontinuity with different flow parameters in a one-dimensional flow field. And then the 3rd Section presents a theoretical analysis for the results which shown in Section 2. In Section 4, some two-dimensional examples are given to verify the correctness of the analysis in the 3rd Section. Finally, a brief summary is given in Section 5.

2 One-dimensional contact discontinuity problem

Computational region $[0,10]$ is selected for this test and the grid number is set to be 200. The initial contact discontinuity is located at the point $x = x_d$. The flow field parameters are dimensionless using the downstream sound velocity, and the initial parameter distribution is

$$(\rho,u,p) = \begin{cases} (\rho_1,u,1/1.4), & 0 \le x \le x_d \\ (1,u,1/1.4), & x_d < x \le 1 \end{cases} \tag{1}$$

Then the Mach numbers upstream and downstream the discontinuity are

$$M_1 = u/a_1 \ (a_1 = 1/\sqrt{\rho_1}), \quad M_2 = u$$

From the later calculation results, it can be seen that if there is a non-physical fluctuation in the process of forming the numerical transition layer of the initial discontinuity, its propagation velocity is the characteristic velocity. In order to avoid the outgoing boundary of the disturbance, the initial discontinuity position x_d satisfies the following formula:

$$\left[x_d - (u - a_1)\, t_{stop}\right] \ge 1, \quad \left[x_d + (u+1)\, t_{stop}\right] \le 9$$

For the convenience of calculation, this section takes the calculation termination moment as $t_{stop} = 2.0$ uniformly.

According to the upstream and downstream Mach numbers of the discontinuities, we set the following five cases, and their specific parameters are shown in Table 1.

Table 1 Initial conditions for different cases

	ρ_1	u	x_d	M_1	M_2
Case1	4.0	0	3.5	0	0

Case2	4.0	2.0	2.0	4.0	2.0
Case3	4.0	0.8	2.0	1.6	0.8
Case4	0.1	2.0	3.0	0.64	2.0
Case5	4.0	0.4	3.5	0.8	0.4

The first-order upwind scheme is selected for numerical calculation in order to avoid the influence of difference scheme and limiter and other factors, and correspondingly, the first-order display time scheme is used for time integration. For all numerical tests, the CFL number is chosen to be 0.5 , and VanLeer, Roe, and AUSM+ are utilized for flux splitting, one for each of the three kinds of splitting schemes.

The distribution curves of flow field parameters, including density, velocity and pressure, for Case1, Case2 and Case3 are given in Figure 1, Figure 2 and Figure 3, respectively. The distribution of flow field parameters for Case4 and Case5 are similar to that of Case3, with only numerical differences, and are not given here.

From Figure 1, it can be seen that in the stationary flow field, the FDS scheme and the hybrid scheme can keep the contact discontinuity intact, and the density, velocity and pressure parameter distribution curves all keep the initial state. In contrast, in the results of FVS scheme, not only the density profile diffuses at the discontinuity, but also the velocity and pressure curve produces three fluctuations distributed at the discontinuity and on both sides of the discontinuity.

As can be seen in Figure 2, the numerical simulation results of the three flux splitting schemes for the contact discontinuity are the same under the full-field supersonic conditions, with only density dissipation and no change in the velocity and pressure parameters.

It can be seen from Figure 3 that in the presence of a subsonic region in the flow field, the contact discontinuities captured by FDS scheme and hybrid scheme have only variations of density, while the contact discontinuity captured in FVS scheme also has variations of velocity and pressure parameters. The fluctuation profiles are similar to the results in the stationary flow field, where not only fluctuations are present at the discontinuity, but also two nonphysical fluctuations are generated on both sides of the discontinuity. However, although the contact discontinuities calculated in FVS scheme have velocity and pressure variations, their density curves almost coincide with those calculated in FDS scheme and hybrid scheme.

According to the above results, it is considered that for one-dimensional contact discontinuity, the FDS scheme and the hybrid scheme have no dissipation in the stationary flow field and only dissipation of density in the non-stationary flow field. The FVS scheme has density dissipation in all flow fields, but the two non-physical fluctuations with characteristic velocities $u - a_1$ and $u + a_2$ respectively(see Figure 4), which are gradually moving away from the discontinuity, should not be attributed to the numerical dissipation of the FVS scheme because the numerical dissipation serves to "smooth out" the discontinuity, while these two non-physical fluctuations have no effect on the transition zone of the density curve.

In summary, it is considered that the numerical dissipation of the flux splitting scheme is greatly affected by the flow field parameters, and it is difficult to give a strict definition. The non-physical fluctuations caused by the FVS scheme during the simulation of contact discontinuity are numerical errors, which affect the velocity and pressure parameter distribution of the flow field, which is the reason why the numerical dissipation of the FVS scheme seems to be larger than that of the FDS scheme and the hybrid scheme.

In addition, Figure 5 gives the curve distribution of the relative pressure error of the contact interruptions captured using the fifth-order WENO scheme under Case1 conditions. It can be seen that the high-resolution characteristic of the high-order schemes make it possible to generate a more complex error structure when simulating the contact discontinuities, and there may even be cases where the error extremes are larger than those of the first-order upwind scheme, so the flow field structures appearing in the calculation results of the higher-order schemes should be treated with caution.

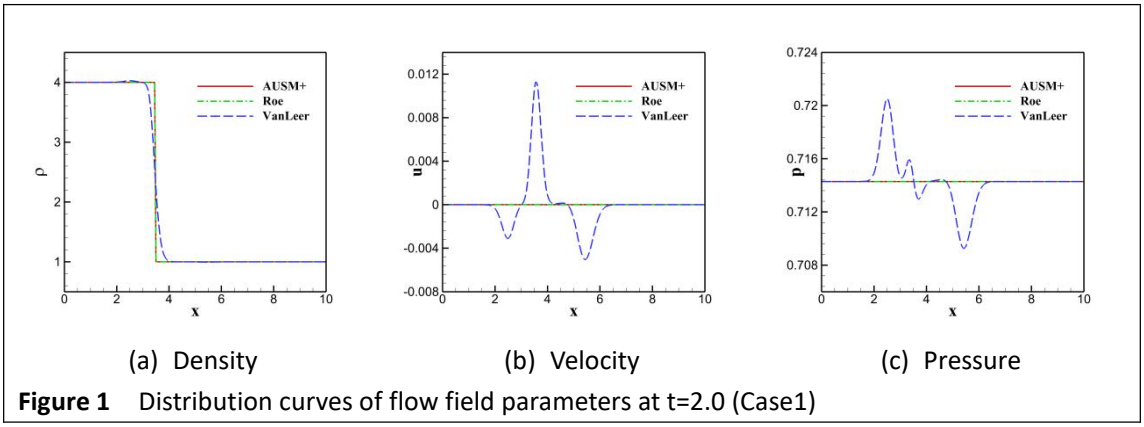

(a) Density (b) Velocity (c) Pressure

Figure 1 Distribution curves of flow field parameters at t=2.0 (Case1)

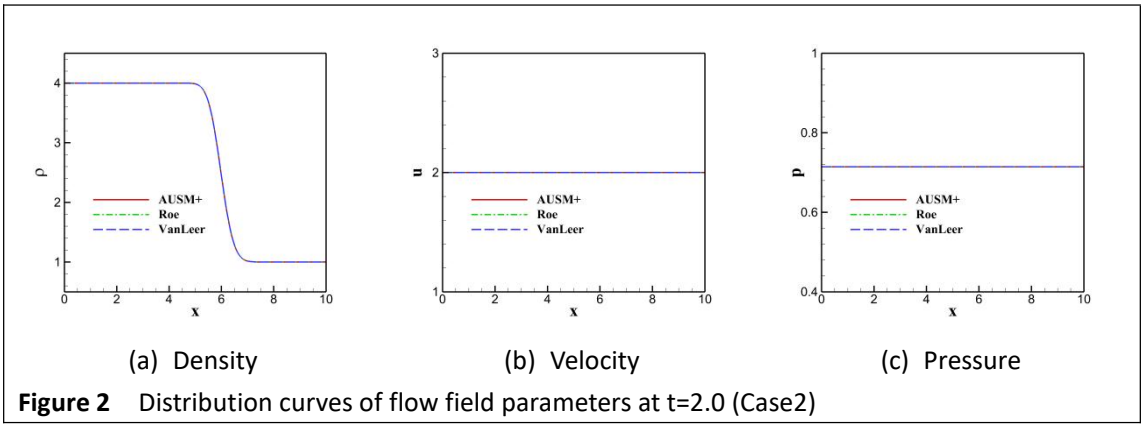

(a) Density (b) Velocity (c) Pressure

Figure 2 Distribution curves of flow field parameters at t=2.0 (Case2)

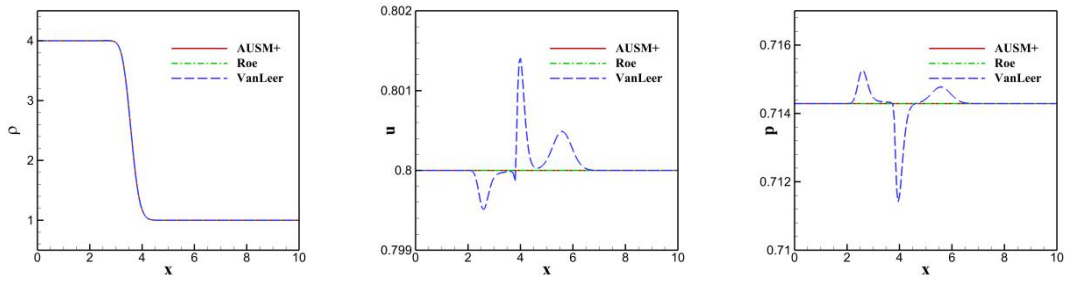

(a) Density (b) Velocity (c) pressure

Figure 3 Distribution curves of flow field parameters at t=2.0 (Case3)

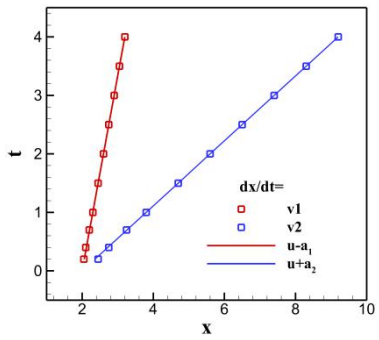

Figure 4 The position-time curves of non-physical waves

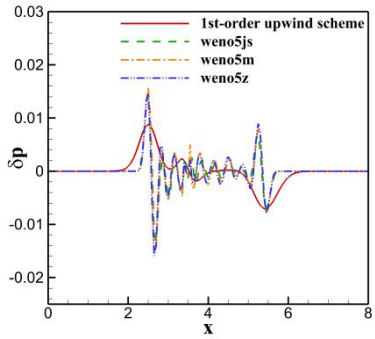

Figure 5 Pressure relative error curves for different formats(a third-order total variation diminishing Runge-Kutta scheme is used for time integration for the WENO schemes, and the VanLeer scheme is utilized for flux splitting)

3 Theoretical analysis for the results of different splitting schemes

This section provides a theoretical analysis of the reasons for the different results of different splitting schemes in Section 2 when contact discontinuities are numerically simulated.

3.1 Theoretical analysis for the results of the FDS scheme

During the calculation, the initial discontinuity satisfying Euler's equation changes from a mathematical discontinuity to a numerical transition zone, and the numerical solution in finite difference scheme satisfies the following modified equation in the transition zone according to CFD theory:

$$\frac{\partial U}{\partial t}+\frac{\partial F}{\partial x}=\sum_{n=2}^{\infty}\gamma_n\frac{\partial^n U}{\partial x^n} \tag{2}$$

As shown in Figure 6, since a single grid point cannot store two sets of data, the initial discontinuity must occupy two grid points. Assuming that the center of the initial discontinuity is at the half-point $i+1/2$ (also known as the interface), then the initial flow field parameters at point i are equal to those at point $i-1$. For FDS

schemes, the following equation is obtained after discretizing the Euler's equation.

$$U_i^{n+1} = U_i^n - \frac{\Delta t}{\Delta x}\left(H_{i+1/2}^n - H_{i-1/2}^n\right) \tag{3}$$

Taking the Roe scheme as an example, the flow field parameters stored on the grid points are used to reconstruct the interfacial fluxes with the first-order accuracy written as:

$$H_{i+1/2} = \frac{1}{2}\left[\left(F_{i+1} + F_i\right) - A^*\left(U_{i+1} - U_i\right)\right], \quad H_{i-1/2} = \frac{1}{2}\left(F_i + F_{i-1}\right) = F_i$$

Where the generalized coefficient matrix A^* is obtained after calculating the interface vector U^* using the Roe averaging formula. The parameters on both sides of the contact discontinuity satisfy the condition of u_{i+1}=$u_i = u^*$ and p_{i+1}=$p_i = p^*$, and it shows that the amount of interfacial density change has no effect on the momentum and energy equations:

$$\Delta F^* = A^*\left(U_{i+1} - U_i\right) = \left[-\left(\Delta\rho\right)u^*, 0, 0\right]^T, \quad \Delta\rho = \rho_{i+1} - \rho_i$$

The flow field parameters after one time step are calculated as

$$\begin{pmatrix} \rho \\ \rho u \\ 0.5\rho u^2 + p \end{pmatrix}_i^1 = \begin{pmatrix} \rho \\ \rho u \\ 0.5\rho u^2 + p \end{pmatrix}_i^0 - \frac{u^0 \Delta t}{\Delta x}\begin{pmatrix} 1 \\ u \\ 0.5u \end{pmatrix}^0 \Delta\rho \tag{4}$$

From Equation (4), it can be seen that for a stationary flow field with the initial velocity $u^0 = 0$, the flow field parameters remain constant after one time step. For the flow field with the initial velocity $u^0 \neq 0$, the density changes during the time advance because the density is not equal on both sides of the initial discontinuity, i.e., $\Delta\rho \neq 0$. But equations $u_i^1 = u_i^0$ and $p_i^1 = p_i^0$ can be introduced after bringing the mass equation to the momentum and energy equations. The above explains the properties very well exhibited by the previous simulation of contact discontinuity using the Roe scheme.

In supersonic flow, the disturbance theoretically does not propagate upstream, but according to the above equations, there is also $\rho_i^1 \neq \rho_i^0$ under such conditions, which is obviously unreasonable.

3.2 Theoretical analysis for the results of the FVS scheme

For the FVS scheme, the discrete Euler's equation using the first-order upwind scheme is written in the following uniform form.

$$U_i^{n+1} = U_i^n - \frac{\Delta t}{\Delta x}\left(F_i^+ - F_{i-1}^+ + F_{i+1}^- - F_i^-\right)^n \tag{5}$$

In the supersonic flow with Mach number $M_1 > 1$ and $M_2 > 1$, since the negative flux under supersonic conditions is 0 and the initial flow field parameters at point i are equal to those at point $i-1$, the equation $U_i^1 = U_i^0$ can be obtained, followed by the density parameter equation $\rho_i^1 = \rho_i^0$. Besides, the update of the flow field

parameters at point $i+1$ can be written in the following form.

$$U_{i+1}^1 = U_{i+1}^0 - \frac{\Delta t}{\Delta x}\left(F_{i+3/2}^+ - F_{i+1/2}^+\right)^0$$
$$= U_{i+1}^0 - \frac{\Delta t}{\Delta x}\left(F_{i+1}^+ - F_i^+\right)^0$$

The specific form of the above equation is

$$\begin{Bmatrix}\rho\\ \rho u\\ \rho e\end{Bmatrix}_{i+1}^1 = \begin{Bmatrix}\rho\\ \rho u\\ \rho e\end{Bmatrix}_{i+1}^0 - \frac{\Delta t}{\Delta x}\left(\begin{Bmatrix}\rho u\\ \rho u^2+p\\ (\rho e+p)u\end{Bmatrix}_{i+1}^0 - \begin{Bmatrix}\rho u\\ \rho u^2+p\\ (\rho e+p)u\end{Bmatrix}_{i}^0\right)$$

After one time step, although there is a change in the conserved variables at point $i+1$, resulting in $U_{i+1}^1 \neq U_{i+1}^0$, bringing the density $\rho_{i+1}^1 = \rho_{i+1}^0 - \frac{\Delta t}{\Delta x}\left(\rho_{i+1}^0 - \rho_i^0\right)u_{i+1}^0$ into U_{i+1}^1 yields the equations $p_{i+1}^1 = p_{i+1}^0$ and $u_{i+1}^1 = u_{i+1}^0$. The above analytical results are consistent with the property that the perturbations of hyperbolic equations do not propagate upstream, and the results in the FVS scheme is more reasonable than those in the Roe scheme in this regard.

Consider a stationary flow field with Mach number $M_1 = M_2 = 0$, the negative flux on both sides of the discontinuity satisfies the equation $F_{i+1}^- \neq F_i^-$, so the conserved variables change after one time step, resulting in $U_i^1 \neq U_i^0$. Since there is a nonlinearity between the speed of sound and the pressure and density in the flux splitting expression, bringing $\rho_i^1 \neq \rho_i^0$ into U_i^1 gives $u_i^1 \neq u_i^0$ and $p_i^1 \neq p_i^0$ and likewise $u_{i+1}^1 \neq u_{i+1}^0$ and $p_{i+1}^1 \neq p_{i+1}^0$ at point $i+1$. As a result, velocity and pressure waves propagating to both sides appear in the results of the FVS scheme when numerically simulating a contact discontinuity in a stationary flow field. This effect is also present when one or both sides of the discontinuity are subsonic.

3.3 Theoretical analysis for the results of the hybrid scheme

For the hybrid scheme AUSM+, the interfacial flux can be written as

$$F_{i+1/2} = c_{i+1/2} Ma_{i+1/2} \Phi_{i+1/2} + p_{i+1/2} \tag{6}$$

Focus on the update of the flow field parameters at point $i+1$. When the velocity of the flow field is 0, the Mach number of the half point is $Ma_{i+1/2} = 0$. Then the flow field parameters satisfy the equation $U_{i+1}^1 = U_{i+1}^0 - \frac{\Delta t}{\Delta x}\left(F_{i+3/2}^0 - F_{i+1/2}^0\right) = U_{i+1}^0 - 0 = U_{i+1}^0$ under the condition of equal pressure in

the whole field, so the AUSM+ scheme can keep the parameters of the stationary flow field unchanged. When the velocity of the flow field is not 0, the density of point $i+1$ changes in the process of calculation, but the updated density ρ_{i+1}^1 can be brought into U_{i+1}^1 to obtain the equations $p_{i+1}^1 = p_{i+1}^0$ and $u_{i+1}^1 = u_{i+1}^0$. The supersonic flow field is taken as an example to illustrate this. When the flow field is supersonic, the flow field parameters after one time step are as follows:

$$\begin{Bmatrix} \rho \\ \rho u \\ \rho e \end{Bmatrix}_{i+1}^1 = \begin{Bmatrix} \rho \\ \rho u \\ \rho e \end{Bmatrix}_{i+1}^0 - \frac{\Delta t}{\Delta x}\left(c_{i+1}^0 Ma_{i+1}^0 \begin{Bmatrix} \rho \\ \rho u \\ \rho e + p \end{Bmatrix}_{i+1}^0 + \begin{Bmatrix} 0 \\ p \\ 0 \end{Bmatrix}_{i+1}^0 - c_i^0 Ma_i^0 \begin{Bmatrix} \rho \\ \rho u \\ \rho e + p \end{Bmatrix}_i^0 - \begin{Bmatrix} 0 \\ p \\ 0 \end{Bmatrix}_i^0 \right)$$

where the updated density is $\rho_{i+1}^1 = \rho_{i+1}^0 - \frac{\Delta t}{\Delta x}\left(\rho_{i+1}^0 - \rho_i^0\right)u_{i+1}^0$, and the following equation can be obtained by substituting it into the momentum equation:

$$u_{i+1}^1 = \frac{(\rho u)_{i+1}^0 - \frac{\Delta t}{\Delta x}\left(u_{i+1}^0 (\rho u)_{i+1}^0 + p_{i+1}^0 - u_i^0 (\rho u)_i^0 + p_i^0\right)}{\rho_{i+1}^0 - \frac{\Delta t}{\Delta x}\left(\rho_{i+1}^0 - \rho_i^0\right)u_{i+1}^0}$$

In the above equation, since $p_{i+1}^0 = p_i^0$ and $u_{i+1}^0 = u_i^0$, we have

$$\begin{aligned} u_{i+1}^1 &= \frac{u_{i+1}^0 \rho_{i+1}^0 - u_{i+1}^0 \frac{\Delta t}{\Delta x}\left(\left(\rho_{i+1}^0 - \rho_i^0\right)u_{i+1}^0\right)}{\rho_{i+1}^0 - \frac{\Delta t}{\Delta x}\left(\rho_{i+1}^0 - \rho_i^0\right)u_{i+1}^0} \\ &= u_{i+1}^0 \end{aligned}$$

Similarly, $p_{i+1}^1 = p_{i+1}^0$ can be obtained by bringing ρ_{i+1}^1 and u_{i+1}^1 into the energy equation.

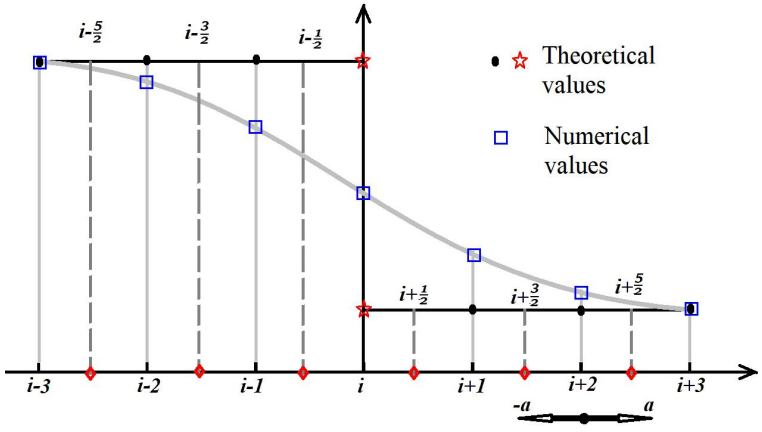

Figure 6 Distribution of flow parameters within the region of discontinuity and transition zones

4 Numerical tests for veritying the theoretical analysis

4.1 Two-dimensional flow within one contact discontinuity

In the two-dimensional problem, the initial contact discontinuity is placed in a flow field with supersonic velocity in the x-direction. Computational region $[0,2]\times[-2,2]$ is selected for this test and the grid number is set to be 200×400. For all the cases in this section, the calculations were first performed using the first-order upwind scheme, and the results show that the flow field is maintained when the flux splitting scheme is used in either FDS or hybrid scheme. Therefore, only the results of calculations using the VanLeer scheme are given in this section. The third-order strongly stable Runge-Kutta scheme[23] with $CFL=0.5$ is used for time integration.

The initial contact discontinuity is located along the line $y=0$, and the initial conditions are given by

$$(\rho,u,v,p)=\begin{cases}(\rho_1,u_1,v,p), & 0\le y\le 2;\\ (\rho_2,u_2,v,p), & -2\le y<0.\end{cases} \tag{6}$$

where $\rho_1=4$, $\rho_2=1$, $u_1=u_2=2$, $v=0$, $p=1/1.4$.

Figure 7 gives the pressure relative error contours and vorticity contours for this case at the calculation time $t=1.5$. The initial velocity of the flow field is constant and the vorticity is 0, so the contours of the vorticity distribution given in Fig. 7 also represents the error distribution of the flow field. It can be seen the VanLeer scheme cannot keep the discontinuity properly in the calculation process, and errors will be generated on both sides of the discontinuity. The generated errors are propagated to both sides along the y-direction with the local sound velocity, and the error distribution range with the boundary of the characteristic line is formed under the action of the supersonic flow in the x-direction.

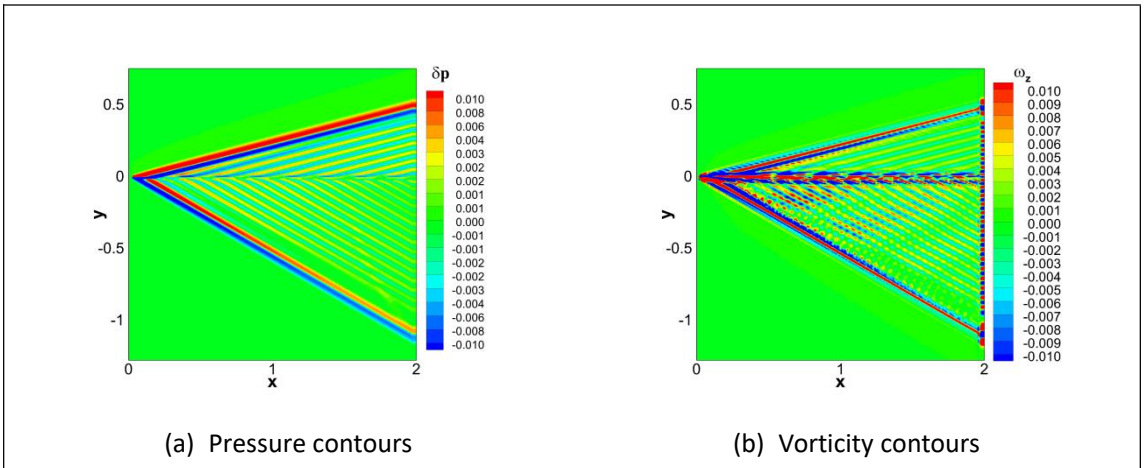

(a) Pressure contours (b) Vorticity contours

Figure 7 Flow field parameter contours at t=1.5(the 5th-order WENOZ scheme is used)

4.2 Two-dimensional flow within double contact discontinuities

We further designed the flow field with two discontinuities at the same time. The initial flow field parameters are set as follows

$$(\rho,u,v,p)=\begin{cases}(\rho_1,u_1,v,p), & -0.1\le y\le 0.1;\\ (\rho_2,u_2,v,p), & else.\end{cases} \tag{7}$$

where $\rho_1=4.0$, $\rho_2=1.0$, $u_1=u_2=2.0$, $v=0$, $p=1/1.4$.

Figure 8 gives pressure error distribution contours and vorticity contours for this case at the calculation time $t=1.5$. From the figure, it can be seen that the errors generated by the two discontinuities change the error distribution range of each discontinuity in the process of interfering with each other, and complex small-scale structures are generated. This further proves that the discontinuities calculated in the FVS scheme change from initial mathematical discontinuity to numerical shear layer with thicknesses during the solution of the supersonic flow field, which inevitably induce nonphysical structures that interfere with each other.

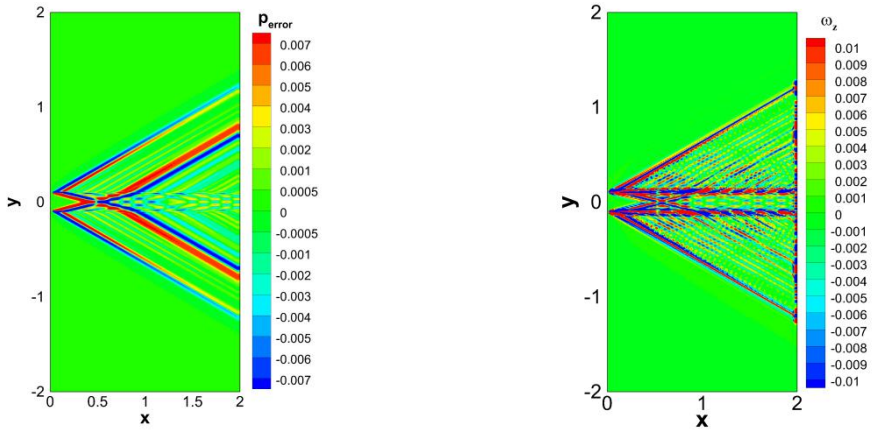

(a) Pressure contours (b) Vorticity contours

Figure 8 Flow field parameter contours at t=1.5(the 5th-order WENOZ scheme is used)

In the literature, CFD researchers often use the 2-D Riemann problems[15] as numerical test cases to express the magnitude of numerical dissipation of the flux splitting scheme. Taking Configuration 6 as an example, it is often considered that the scheme with richer small-scale flow structures near the contactlines has lower numerical dissipation. However, it can be seen from Figure 7 and Figure 8 that the non-physical fluctuations interfering with each other when the FVS scheme captures the contact discontinuities can also produce complex small-scale structures, so the fluctuations in the calculation results should be treated with caution when using high order finite difference schemes.

5 Summary

By discussing the results of the above numerical calculations and analyzing their mechanism, we can draw the following conclusions in response to the questions posed in the introduction.

Firstly, in the numerical simulation of contact discontinuity, the numerical

dissipation characteristics of three kinds of flux splitting schemes, such as the FVS scheme, the FDS scheme and hybrid scheme, are affected by the initial parameter distribution of the flow field, and the numerical dissipation of the schemes behave differently under different flow field parameter conditions, so a strict definition cannot be given. In the stationary flow field, the FDS and hybrid schemes have no numerical dissipation, and the FVS scheme has only density dissipation. In non-stationary flow fields, all three flux splitting schemes have only density dissipation, and the magnitude of the density dissipation is consistent. In particular, for the flow field with subsonic region, the FDS and hybrid schemes are able to keep the flow field pressure and velocity constant, while the results calculated in the FVS scheme produce pressure and velocity waves, which propagate outward at characteristic velocities and the range of influence varies with time, so it is considered that these non-physical velocity and pressure waves do not belong to the scope of numerical dissipation, but are only numerical errors.

In addition, the low dissipation and high resolution characteristics of the higher-order differential schemes can well preserve the non-physical waves generated by the FVS scheme, leading to the anomaly that the error in the calculation results of the higher-order differential scheme is larger than that of the first-order upwind scheme. And in multidimensional flow fields, non-physical fluctuations in different directions generated by the FVS scheme interfere with each other to produce more complex non-physical structures. Therefore, the use of high-order schemes in such cases should be cautious about the fluctuation phenomena appearing in the calculation results.

Acknowledgements

The work in this paper is supported by the National Numerical Wind Tunnel project (NNW2018-ZT4B09).

Authors' contributions

All authors read and approved the final manuscript.

Funding

The work in this paper is supported by the National Numerical Wind Tunnel project (NNW2018-ZT4B09).

Availability of data and materials

All data and materials are available from the authors of this paper.

Competing interests

The authors declare that they have no competing interests.

Author details

School of Aeronautic and Astronautics, Dalian University of Technology , 116024 Dalian, China

References

1. Zhang HB, Zhang F, Liu J, McDonough JM, Xu CG(2020) A simple extended compact nonlinear scheme with adaptive dissipation control. Communications in Nonlinear Science and Numerical Simulation 84
2. Hu Z, Zhang XY, Cui WC, Wang F, Li XW, Li Y(2020) A simple method of depressing numerical dissipation effects during wave simulation within the Euler model. Acta Oceanologica Sinica 39(1)
3. Kalita P, Dass AK, Hazarika J(2020) A new approach for numerical-diffusion control of flux-vector-splitting schemes for viscous-compressible flows. International Journal of Numerical Methods for Heat & Fluid Flow 31(1)
4. Yan C, Zhang Z, Zhang LX, Xu ZG(2003) Performance Analysis of upwind schemes. Acta Aerodynamica Sinica 3:336-341
5. Steger JL, Warming RF(1981) Flux vector splitting of the inviscid gas dynamics equations with application to finite difference methods. Journal of Computational Physics 40(2):263-93
6. van Leer B(1981) Flux vector splitting for Euler equations. Lecture Notes in Physics 170
7. Roe PL(1981) Approximate Riemann solvers, parameter vectors and difference schemes. Jounal of computational physics 43
8. Toro EF, Spruce M, Speares W(1994) Restoration of the contact surface in the HLL-Riemann solver. Shock Waves 4:25-34
9. Kitamura K, Shima E. A new pressure flux for AUSM-family schemes for hypersonic heating computations. Hawaii: 20th AIAA Computational Fluid Dynamics Conference 2011
10. Edwards JR(1997) A low-diffusion flux-splitting scheme for Navier-Stokes calculations. Computers & Fluids 26(6):635-659
11. Sod GA(1978) A survey of several finite difference methods for systems of nonlinear hyperbolic conservation laws. Journal of Computational Physics 27(1):1-31
12. Lax PD(1954) Weak solutions of nonlinear hyperbolic equations and their numerical computation. Communications on Pure and Applied Mathematics 7(1):15-193
13. Shu CW, Osher S(1989) Efficient implementation of essentially non-oscillatory shock-capturing schemes. Journal of Computational Physics 83(1):32-78
14. Lax P, Liu X(1998) Solution of two-dimensional Riemann problems of gas dynamics by positive schemes. Siam Journal on Scientific Computing 19(2):319-340
15. Liu J, Han F(2020) Discussions on two problems in applications of high-order finite difference schemes. Acta Aerodynamica Sinica 38(2):244-253
16. Liu J, Han F, Wei YX(2020) Discussions on the numerical errors of high-order WENO schemes under some specific conditions. Acta Aeronautica et Astronautica Sinica 42(8):124940
17. Zou DY, Xu CG, Dong HB, Liu J(2017) A shock-fitting technique for cell-centered finite volume methods on unstructured dynamic meshes. Journal of Computational Physics, 345:866-882
18. Chang SY, Bai XZ, Cui XQ, Liu J(2020) An improved unsteady shock-fitting algorithm. Acta Aeronautica et Astronautica Sinica 41(2):163-176

Figures

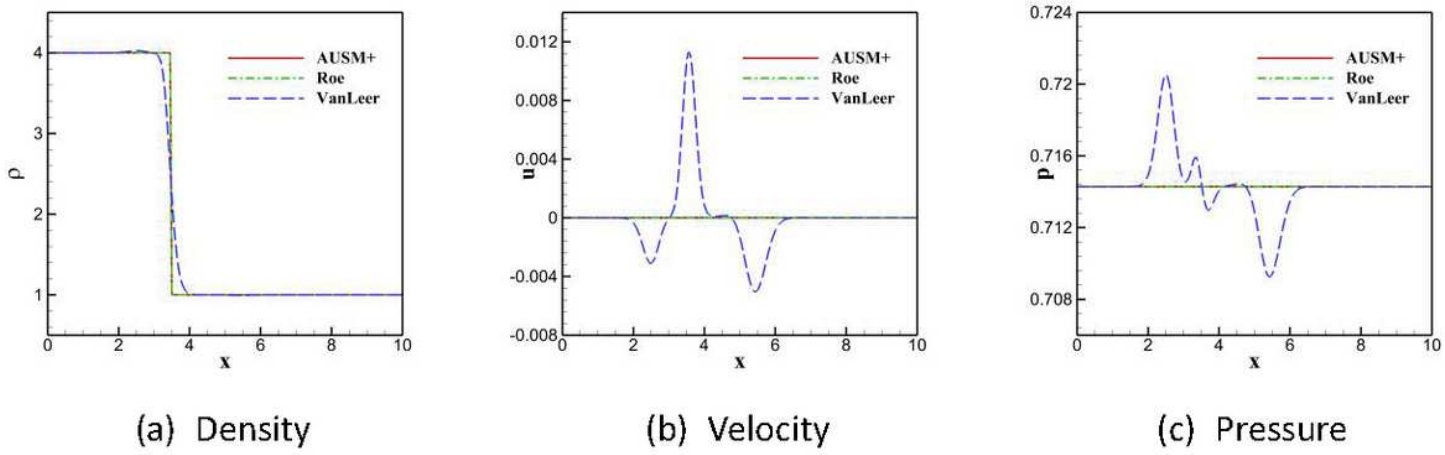

Figure 1

Distribution curves of flow field parameters at t=2.0 (Case1)

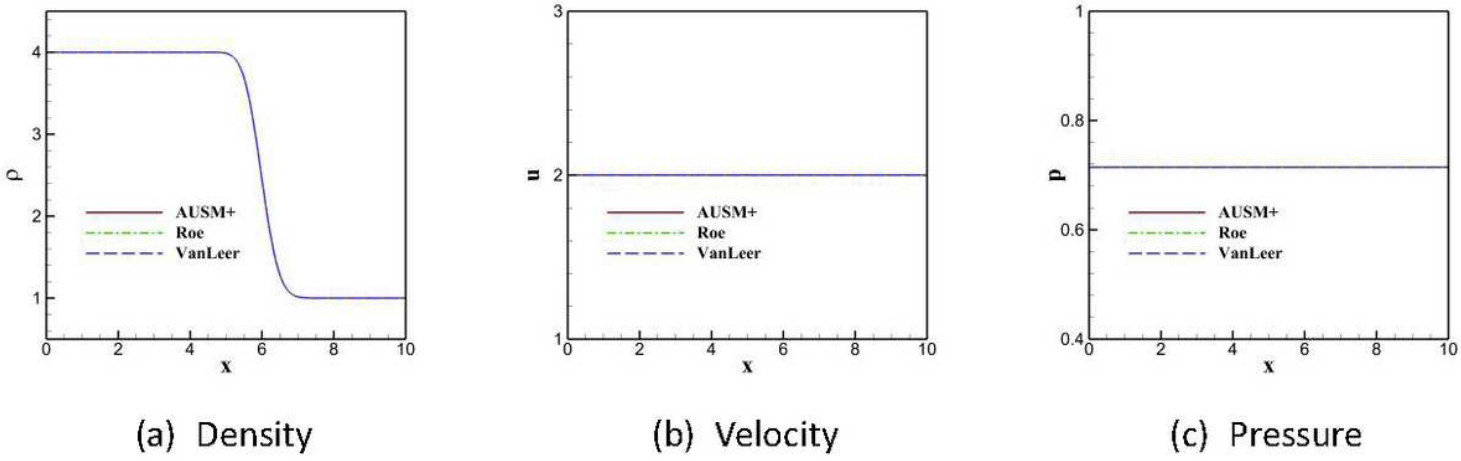

Figure 2

Distribution curves of flow field parameters at t=2.0 (Case2)

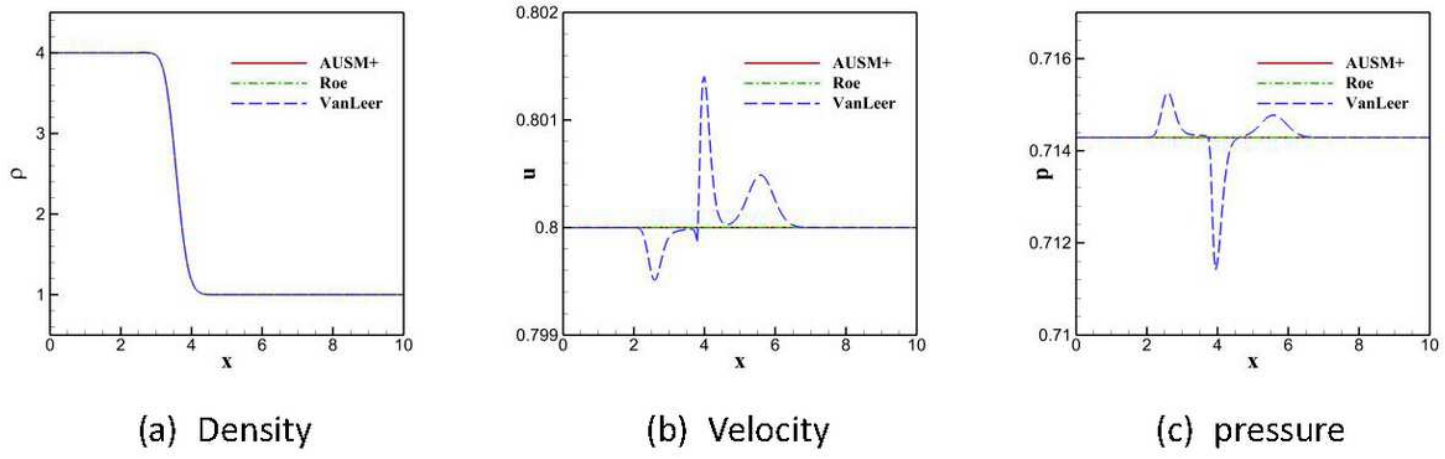

Figure 3

Distribution curves of flow field parameters at t=2.0 (Case3)

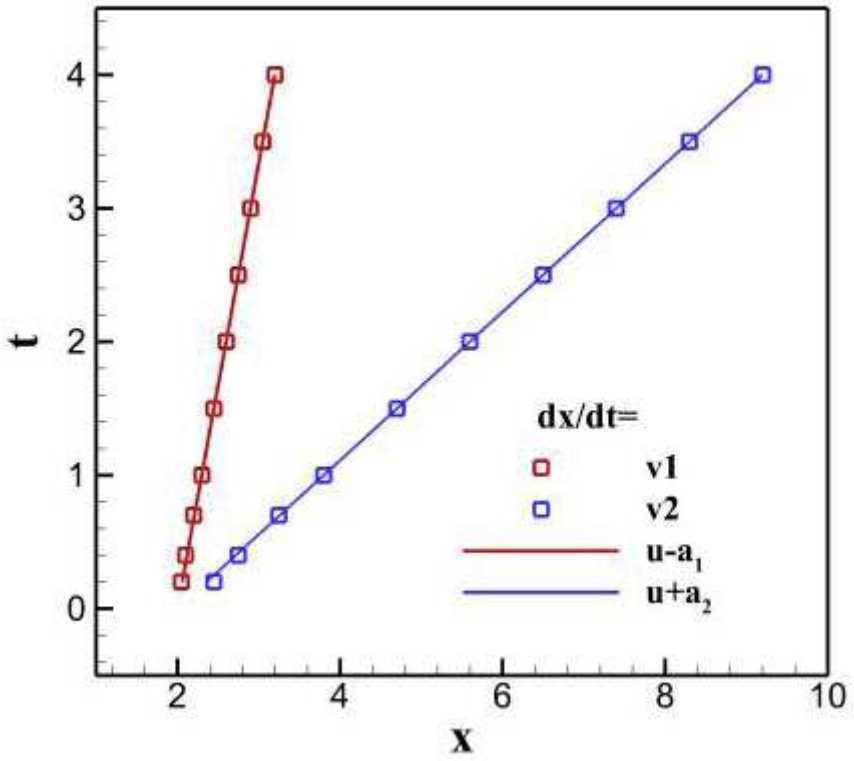

Figure 4

The position-time curves of non-physical waves

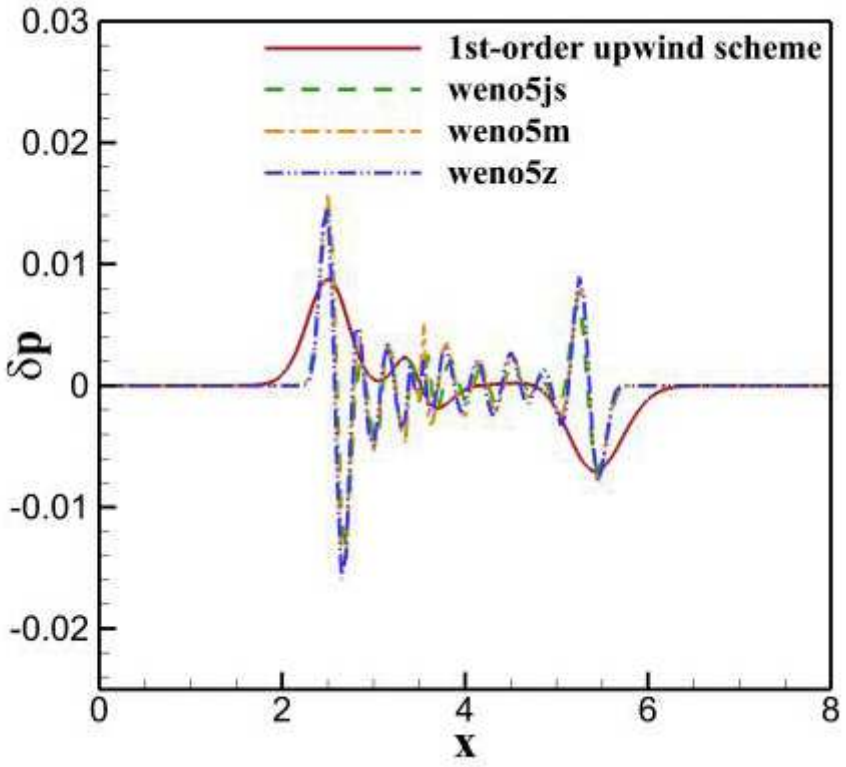

Figure 5

Pressure relative error curves for different formats(a third-order total variation diminishing Runge-Kutta scheme is used for time integration for the WENO schemes, and the VanLeer scheme is utilized for flux splitting)

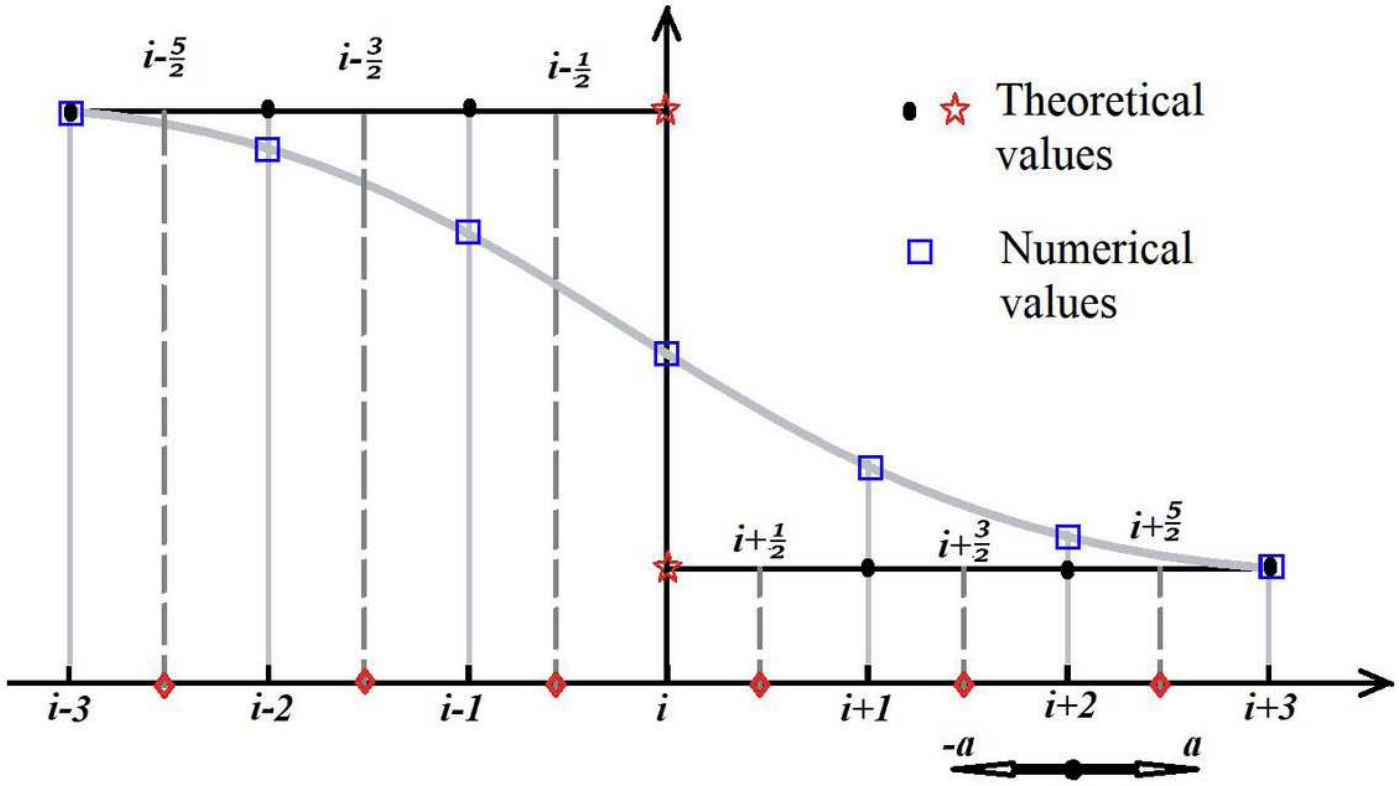

Figure 6

Distribution of flow parameters within the region of discontinuity and transition zones

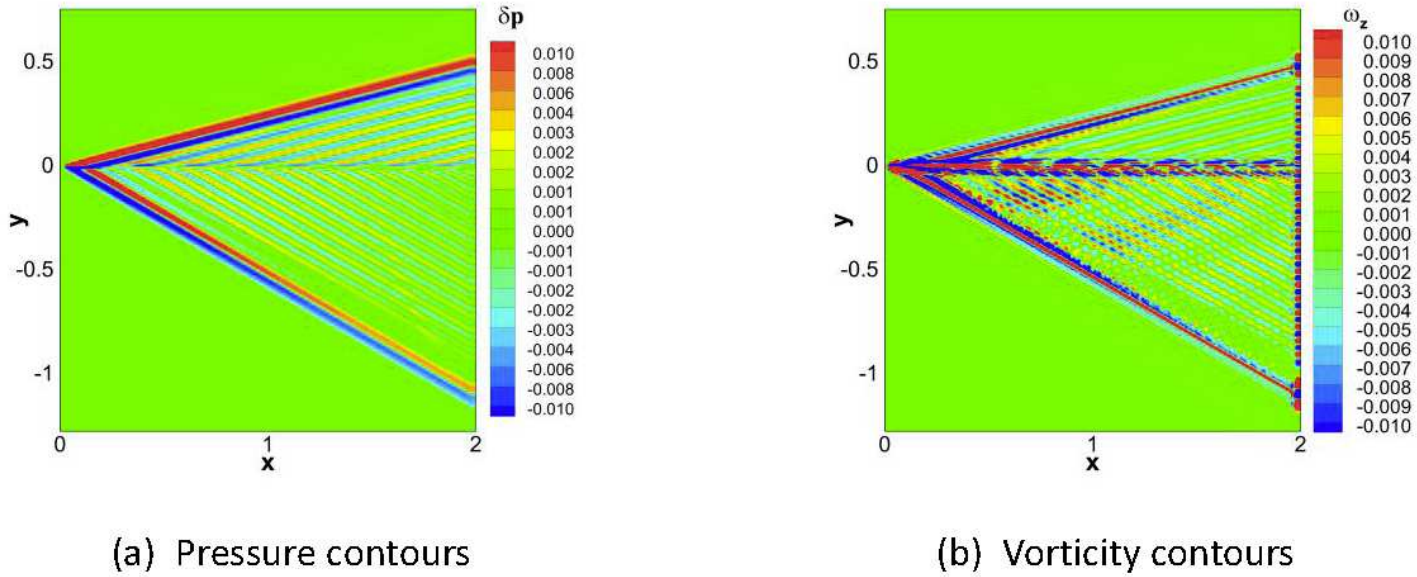

Figure 7

Flow field parameter contours at t=1.5(the 5th-order WENOZ scheme is used)

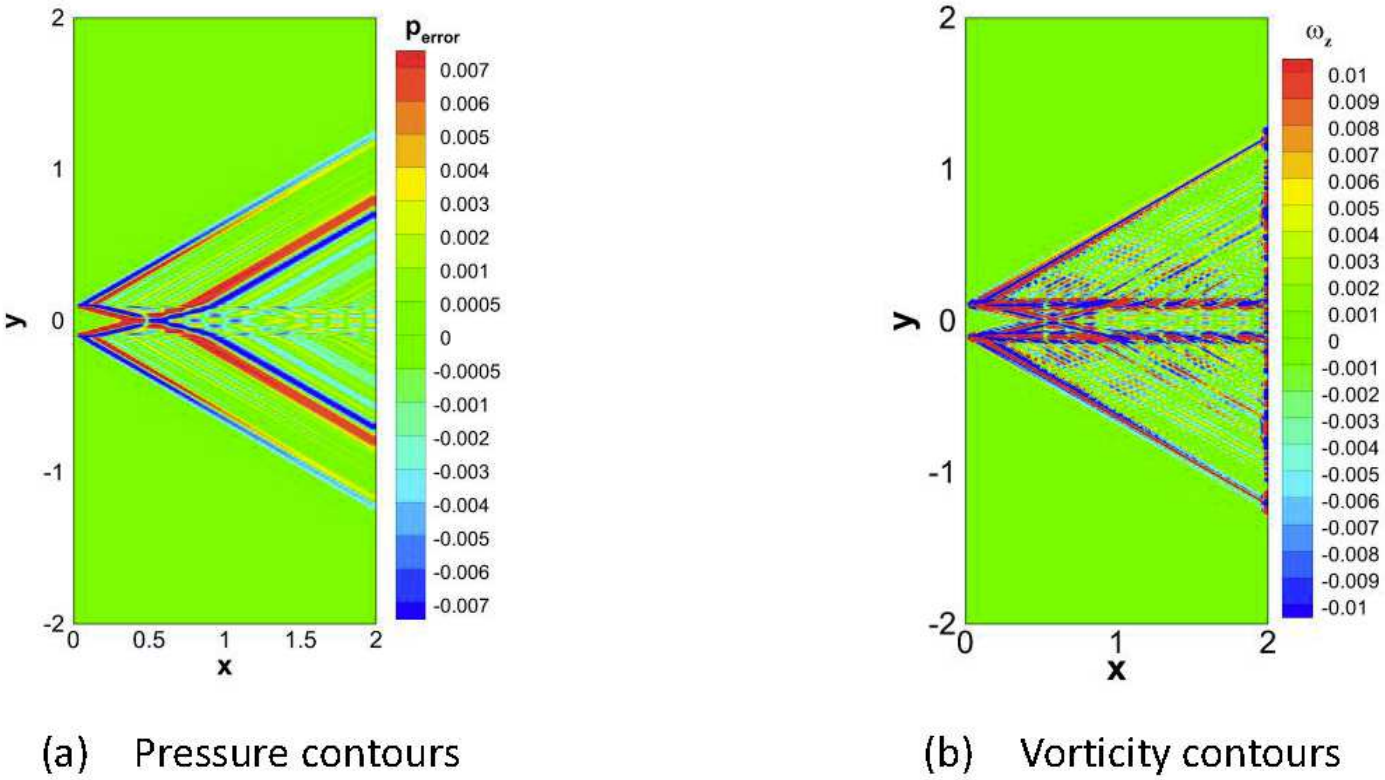

Figure 8

Flow field parameter contours at t=1.5(the 5th-order WENOZ scheme is used)